J. Biochem. 2012;151(5):541–549 doi:10.1093/jb/mvs023

JB THE JOURNAL OF BIOCHEMISTRY

Crystal structure of non-phosphorylated MAP2K6 in a putative auto-inhibition state

Received December 8, 2011; accepted January 27, 2012; published online March 1, 2012

Takashi Matsumoto[1,2,*†], Takayoshi Kinoshita[2], Hitomi Matsuzaka[1,†], Ryoko Nakai[3], Yasuyuki Kirii[3], Koichi Yokota[3] and Toshiji Tada[2]

[1]PharmAxess, Inc., 3-9-12, Matsubara-cho, Akishima, Tokyo 196-8666; [2]Department of Biological Science, Graduate School of Science, Osaka Prefecture University, Gakuencho 1-1, Naka-ku, Sakai, Osaka 599-8531; and [3]Carna Biosciences, Inc., BMA 3F 1-5-5 Minatojima-Minamimachi, Chuo-ku, Kobe 650-0047, Japan

*Takashi Matsumoto, Rigaku Corporation., 3-9-12, Matsubara-cho, Akishima, Tokyo 196-8666, Japan. Tel: +81-42-545-8166, Fax: +81-42-545-8158, email: t-matumo@rigaku.co.jp

†Present address: Takashi Matsumoto/Hitomi Matsuzaka, Rigaku Corporation., 3-9-12, Matsubara-cho, Akishima, Tokyo 196-8666, Japan

Mitogen-activated protein kinase kinase 6 (MAP2K6) plays a crucial role in the p38 MAP kinase signal cascade that regulates various stress-induced responses and is associated with pathological conditions. The crystal structure of human non-phosphorylated MAP2K6 (npMAP2K6) complexed with an ATP analogue was determined at 2.6 Å resolution and represents an auto-inhibition state of MAP2K6. Three characteristics of short α-helices configured in the activation loop region, termed activation helices (AH1, AH2 and AH3), are important in controlling the auto-inhibition mechanism. AH1 displaces the αC-helix, a component essential for forming the active configuration, away from the active site. AH1 and AH2 were found to enclose the γ-phosphate, the leaving group of ATP. A comparison with the related enzymes, MAP2K1 and MAP2K4 reveals that MAP2K6 has the unique auto-inhibition mechanism mediated by the three activation helices.

Keywords: activation helices/auto-inhibition state/MAP2K6/MAP2K/X-ray crystal structure.

Abbreviations: AMP-PNP, adenylyl-imidodiphosphate; ATP, adenosine triphosphate; DLS, dynamic light scattering; DTT, dithiothreitol; DVD, domain for versatile docking; ERK, extracellular signal-regulated kinase; MAP, mitogen-activated protein; MAPK, MAP kinase; MAP2K, MAP kinase kinase; MAP3K, MAP kinase kinase kinase; NRD, negative regulatory domain; RMSD, root-mean-square deviation; SDS, sodium dodecyl-sulfate; PAGE, polyacrylamide gel electrophoresis.

Mitogen-activated protein (MAP) kinase cascades provide an important connection between external stimuli and activation of intracellular signalling, and are mainly organized as three sequentially tiered kinases referred to as MAP kinase kinase kinase (MAP3K), MAP kinase kinase (MAP2K) and MAP kinase (MAPK). The four human MAP kinase cascades are identified as the extracellular signal-regulated kinase 1/2 (ERK1/2) and their activators MAP2K1 and MAP2K2, ERK5 and its activator MAP2K5, c-Jun N-terminal kinase (JNK) isoforms and their activators MAP2K4 and MAP2K7, and p38 MAP kinase isoforms and their activator MAP2K3 and MAP2K6 (*1*, *2*).

MAP2K6 plays a crucial role in the p38 MAP kinase cascade that is activated by pro-inflammatory cytokines, bacterial lipopolysaccharides, UV, heat shock or osmotic stress (*3*–*5*). The activated cascade facilitates the production of cytokines, cell differentiation, proliferation and apoptosis (*6*–*9*). Dysfunction of this cascade is associated with pathological inflammation and ovarian cancer (*10*). MAP2K6 is activated by MAP3K3 through dual phosphorylation events on Ser207 and Thr211 in the activation loop (*11*–*15*) In turn, MAP2K6 activates all p38 MAP kinase isoforms through dual phosphorylation of threonine and tyrosine in the Thr–Gly–Tyr sequence located in the activation loop; however, MAP2K6 does not activate other MAP kinases (*16*–*18*). In other words, the MAP2K6/p38 MAP kinase cascade functionally makes no crosstalk with the other cascades. The fidelities in these signalling cascades are enabled by the allosteric interactions with the upstream or downstream kinases. The domain for versatile docking (DVD domain) in the C-terminus and the docking domain (D domain) located at the N-terminus of MAP2K6 mediate the interactions with MAP3K3 and all p38 isoforms, respectively (*19*–*21*).

Each kinase, including MAP2Ks, possesses molecular machinery that strictly regulates its activity, and involves a conformational change induced by phosphorylation and/or the activator binding. The most important structural elements necessary for the inactive-to-active transition of kinases are rearrangements of the αC-helix and the activation loop region. For example, the Akt crystal structures showed that the interaction of His196 in the αC-helix with the phosphorylated Thr309 in the activation loop facilitates the αC-helix movement towards the ATP binding pocket, and the activation loop adopts a stretched conformation that functions as a platform for substrate binding (*22*). The activated

conformation of the kinase also allows the substrate to access the γ-phosphate group of ATP with the destabilized conformation as a transition state. The apo-structure of the kinase domain mutant of MAP2K6 replaced with aspartic acid residues at Ser207 and Thr211 (MAP2K6-DD) has recently been determined as an activated mimetic (*23*). In MAP2K6-DD, the N-terminal lobe is partially unwound and the activation loop region is disordered. These flexibilities allow MAP2K6-DD to make the facile transition to the active conformation.

In contrast to the flexible active conformation, the non-phosphorylated kinase is structurally stabilized in an inactive conformation. Two distinct structural stabilizing mechanisms are observed in the non-phosphorylated state of the MAP2K isoforms, MAP2K1 and MAP2K4 (*24*, *25*). In the inactive state of MAP2K1, the negative regulatory domain (NRD: residues 44–58), which follows the D domain located at the N-terminus and within the first 31 residues, functions as a molecular brake and interferes with the αC-helix rearrangement to the active state conformation via interactions with the N- and C-lobes (*24*). In contrast to the data on MAP2K1, the function of the N-terminal 43 residues of MAP2K6 remains unknown, except for the D domain consisting of the N-terminal 15 residues. In the non-phosphorylated state of MAP2K4, the substrate-derived peptide binds at the allosteric site in the N-lobe and induces the auto-inhibition state, in which the activation loop adopts a characteristic long α-helix, protruding out from the MAP2K4 main body, thereby preventing access of the substrate to the active site (*25*). Thus, the MAP2K isoforms MAP2K1 and MAP2K4 present distinct auto-inhibition machineries.

In order to investigate an inactive/active molecular switch of MAP2K6, we have determined the structure of full-length npMAP2K6 complexed with adenylyl-imidodiphosphate (AMP-PNP) as an ATP analogue (npMAP2K6/AMP-PNP).

Materials and Methods

Expression and purification

Full-length human MAP2K6 was cloned into the pET-22b (+) vector (Novagen) using the NdeI and HindIII sites, incorporating a C-terminal His_6-tag. The non-phosphorylated MAP2K6 (npMAP2K6) protein was overexpressed in BL21(DE3) cells (Novagen), which were grown to an $OD_{600} = 0.6$, and then incubated for 20 h at 25°C with protein expression induced by the addition of 0.1 mmol/l isopropyl-β-D-thiogalactopyranoside (IPTG). Cells were collected by centrifugation, and the cell pellet was washed with cold PBS buffer and stored at −80°C. The cell pellet was thawed on ice and resuspended in the lysis buffer (50 mmol/l Tris–HCl pH 7.5, 5% glycerol and 5 mmol/l 2-mercaptoethanol) and disrupted by sonication on ice. The insoluble material was removed by centrifugation at 12,000*g* for 10 min. The supernatant was loaded onto a chelating Sepharose fast flow column (GE Life Sciences) that was pre-charged with Ni^+ and equilibrated with buffer A (50 mmol/l Tris–HCl pH 7.5, 10% glycerol, 300 mmol/l NaCl and 5 mmol/l 2-mercaptoethanol). The chelating Sepharose column was washed with 10 bed volumes of buffer A, and npMAP2K6 was eluted with buffer A containing 200 mmol/l imidazole. The elution was desalted by three concentration–dilution steps using an ultrafiltration membrane (Millipore) and the material loaded onto the Q-Sepharose Fast Flow column (GE Life Sciences) equilibrated with buffer B [50 mmol/l Tris–HCl pH 7.5, 10% glycerol and 10 mmol/l dithiothreitol (DTT)]. The Q-Sepharose column was washed with three bed volumes of buffer B, and the flow-through fractions containing npMAP2K6 were pooled. The npMAP2K6 was finally purified by cation exchange chromatography using a SP-Sepharose Fast Flow column (GE Life Sciences) equilibrated with buffer B. The column was washed using buffer B supplemented with 60 mM NaCl. The npMAP2K6 fraction was eluted with 250 mM NaCl. All chromatographic steps were carried out at 4°C. The purified npMAP2K6 protein without and with AMP-PNP was analysed by sodium dodecyl–sulphate polyacrylamide gel electrophoresis (SDS–PAGE) and Native–PAGE experiments using 12.5% polyacrylamide gels. Gels were stained with Bio Safe coomassie (Bio-Rad).

Activity assay

The MAP2K6 reactions were carried out in 40 µl volumes containing phosphorylated MAP2K6 (Carna Biociences) or prepared npMAP2K6 (0–100 nmol/l) and 250 nmol/l non-phosphorylated p38α MAPK (Carna Biosciences) in 7.5 mmol/l Tris–HCl pH 7.5, 0.005% Tween-20, 1 mmol/l DTT, 10 mmol/l $MgCl_2$ and 1 mmol/l adenosine triphosphate (ATP) at room temperature. Phosphorylated p38α was probed with anti-phosphor-p38MAPK monoclonal antibody (Cell Signaling Technology) as the primary antibody. The amounts of immunocomplex were detected using chemical luminescence.

Dynamic light scattering evaluation

The particle dispersion of npMAP2K6 at various pH conditions was measured by dynamic light scattering (DLS) analysis. Protein samples of the npMAP2K6 complexed with AMP-PNP (npMAP2K6/AMP-PNP) were prepared as a 1 mg/ml protein solution containing the 20 mmol/l buffering compound adjusted to its respective pH (Table I), containing 100 mmol/l NaCl, 10% glycerol, 10 mmol/l DTT, 0.25 mmol/l AMP-PNP and 0.25 mmol/l $MgCl_2$, and filtered through a 0.2 µm membrane filter before the experiments. The DLS analyses were performed by 12 µl injections of the each sample into the glass cell using a DynaPro-801 instrument (Wyatt Technology) at 20°C. Data analyses were performed with Dynamics V5.0 software (Wyatt Technology).

Crystallization

The final purification buffer was replaced with the DLS-optimized buffer that consisted of 20 mmol/l MES–NaOH pH 6.0, 100 mmol/l NaCl, 10% glycerol and 10 mmol/l DTT. This buffer exchange process was carried out by three concentration–dilution steps using an ultra-filtration device (Millipore). The npMAP2K6 solution was finally concentrated to 20 mg/ml. The npMAP2K6/AMP-PNP solution was prepared by adding AMP-PNP and $MgCl_2$ to the concentrated sample to a final concentration of 5 mmol/l. All crystallization trials were performed by the sitting drop vapour diffusion method at 4 and 20°C. The initial crystallization conditions were screened using the commercial kits Crystal Screens 1 and 2, and the INDEX Screen (Hampton Research). Rod-shaped crystals of npMAP2K6/AMP-PNP were grown at 4°C using the reservoir solution consisting of 20% PEG4000, 10% 2-propanol and 0.1 mol/l Na–HEPES–HCl, pH 7.5.

Structure determination

Crystals were frozen by plunging into liquid nitrogen. Preliminary diffraction data were collected in-house using a Rigaku FR-E^+ generator equipped with a Rigaku R-AXIS VII image plate detector. The high-resolution crystallographic data were also collected at the beamline BL-5A of the Photon Factory, KEK (Tsukuba, Japan) using a Quantum 315 CCD detector (ADSC) at 95 K. The diffraction data were integrated and scaled using the CrystalClear package (Rigaku). Subsequent data manipulation was carried out using the CCP4 program package (*26*). The structure was solved by molecular replacement using the program MolRep (*27*), and the MAP2K1 structure [PDB code 3eqd (*24*)] as a search model. Model building was performed using program Coot (*28*), and model refinement was conducted using the programs Refmac5 (*29*) and Phenix (*30*). Coordinates have been deposited at the Protein Databank with the accession code: 3VN9. Details of the data collection and refinement are summarized in Table II. Structure superposition and root mean square deviation (RMSD) calculations were performed using the program Superpose (*31*). Figures were prepared using the program CCP4mg (*32*).

Table I. Conditions for DLS measurements.

pH	20 mM buffer	Dispersion	Peak width (%)
7.5	Tris–HCl (resultant purification buffer)	poly	95.0
4.0	Na–acetate–HCl	poly	60.2
4.4	Na–acetate–HCl	poly	79.8
5.0	Na–citrate-HCl	poly	71.8
5.4	Na–citrate–HCl	poly	55.0
6.0	MES–NaOH	mono	6.9
6.4	Na–Cacodylate–HCl	poly	52.5
7.0	Na–HEPES–HCl	poly	40.0
7.4	Na–HEPES–HCl	poly	49.1
8.0	Tris–HCl	poly	58.8
8.4	Tris–HCl	poly	51.8
9.0	CAPSO–NaOH	poly	53.3
9.4	CAPSO–NaOH	poly	89.5
10.0	CAPS–NaOH	poly	69.2

All conditions contain 100 mmol/l NaCl, 10% glycerol, 10 mmol/l DTT, 0.25 mmol/l AMP-PNP and 0.25 mmol/l $MgCl_2$.

Table II. Data collection and crystallographic analysis.

X-ray diffraction data	
Space group	$P3_121$
Unit cell (Å)	$a=b=83.46$ $c=101.15$
Observations	112,209
Unique reflections	12,124
Resolutions (Å)	20.00–2.60 (2.69–2.60)
Completeness (%)	93.9 (100.0)
Multiplicity	9.26 (9.72)
I/σ (I)	10.3 (2.1)
R-merge (%)[a]	12.4 (53.9)
Refinement statistics	
Resolution (Å)	20.0–2.60
R-factor (%)	26.4
R-free (%)	28.0
Bond length (Å)	0.030
Bond angle (°)	2.59

The numbers in parentheses are given for the highest resolution shells.
[a]R-merge $=\Sigma_h\Sigma_j|I_{hj} - <I_h>|/\Sigma_h\Sigma_j|I_{hj}|$, where h represents a unique reflection and j represents symmetry-equivalent indices. I is the observed intensity and $<I>$ is the mean value of I.

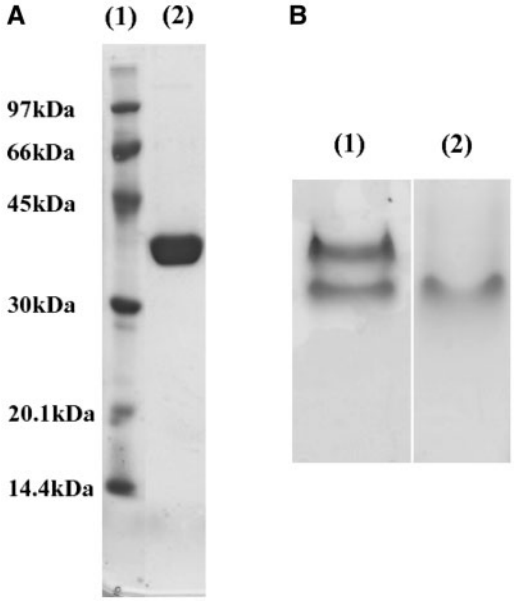

Fig. 1 Image of SDS and Native–PAGE. (A) SDS–PAGE of purified npMAP2K6. The lanes are as follows: lane (*1*), molecular weight marker; lane (*2*), purified npMAP2K6. (B) Native–PAGE analysis separated two bands in the absence of AMP-PNP. The presence of AMP-PNP shifted only the low molecular weight band. (*1*) npMAP2K6 in the absence of AMP-PNP. (*2*) npMAP2K6 in the presence of AMP-PNP.

Results and Discussion

Preparation of npMAP2K6 suitable for crystallization

Optimal soluble expression of MAP2K6 was achieved at 25°C using BL21 (DE3) *Escherichia coli* as an expression host with 0.1 mmol/l IPTG induction and 20 h post-induction incubation. The yield of purified MAP2K6 protein was 15.1 mg from ~3.5 g of cells. The high purity of the target protein was confirmed by SDS–PAGE analysis as a single band of 38 kDa (Fig. 1A). This molecular weight agreed with the theoretical size of 38,315 Da calculated using the amino acids sequence. Nevertheless, Native–PAGE analysis of the protein rendered two clear bands which indicates the presence of distinct surface charges (Fig. 1B), and raises that the possibility that the purified sample contains equal amounts of the phosphorylated and non-phosphorylated MAP2K6. Similar results have been observed previously by us for experiments carried out on Lyn kinase. The purified Lyn sample was detected as four bands on Native–PAGE, therefore displaying the distinct phosphorylation states (*33*). However, the kinase assay experiments revealed that the purified MAP2K6 protein was essentially in the non-phosphorylated state; although the purified sample did display a small amount of activity due to the presence of a trace amount of phosphorylated MAP2K6 detected by western blotting analysis (R. Nakai, unpublished data). Under the assay conditions used, non-phosphorylated MAP2K6 (npMAP2K6) was likely to cause gradual auto-phosphorylation as previously reported (*34*). Furthermore, the addition of the active MAP3K3 conferred hyper activity of purified MAP2K6 because of phosphorylation.

These results indicate that a different factor gives rise to the two bands of npMAP2K6 in the Native–PAGE experiment. Another possibility is that the purified npMAP2K6 in the absence of AMP-PNP is a mixture of monomer and dimer species, whereas in the presence of AMP-PNP the protein adopts a single state. This speculation is supported by the previous analytical gel-filtration studies that showed that the MAP2K6-DD in the absence and presence of ATP formed dimer and monomer species, respectively (*23*). Consequently, the heterogeneous state of purified npMAP2K6 was removed by the addition of AMP-PNP as an ATP analogue (Fig. 1B).

The npMAP2K6/AMP-PNP complex rendered amorphous precipitation with no crystals formed under any conditions examined. Therefore, it was

probable that the protein sample possessed a poly-disperse character with respect to the dynamic molecular radius, and this facilitated aggregation and inhibited crystallization (*35*). DLS analysis of the npMAP2K6/AMP-PNP complex in the final purification buffer showed a highly dispersed distribution of the dynamic molecular radius (Table I). Thus, in order to acquire better conditions, the dynamic molecular radius distribution of the npMAP2K6/AMP-PNP complex was examined using DLS at several pH values over the range of 4.0–10.0 (Table I). The npMAP2K6/AMP-PNP complex formed a monodispersed distribution with a sharp peak when 20 mmol/l MES–NaOH pH 6.0 was used as the buffer. This observation is in keeping with previously reported crystallization conditions used (*36*). Finally, the crystals of the npMAP2K6/AMP-PNP complex were obtained in this optimized buffer condition.

Overall structure of the npMAP2K6/AMP complex

The 2.6 Å resolution crystal structure revealed that the crystallographic asymmetric unit included one npMAP2K6/AMP-PNP complex. The final refinement was converged to an *R*-factor of 26.4% (*R*-free of 28.0%) with reasonable stereochemistry. It was likely that the *R*-factor and *R*-free values were rather high owing to the highest disordered rate. The npMAP2K6 is composed of 340 residues, with 49 residues disordered in the crystal. Although the N-terminal region (residues 1–43) and the His_6-tag were disordered, the kinase domain (residues 44–334) was ordered (Fig. 2A).

The npMAP2K6 structure confers a typical kinase fold, containing a smaller N-terminal lobe (N-lobe) composed of five β-strands and one α-helix (αC-helix) connecting to a larger C-terminal lobe (C-lobe) composed primarily of α-helices. The two lobes are connected via a flexible hinge region. The $F_o - F_c$ omitted map revealed that the AMP-PNP molecule bound in the ATP binding cleft between the two lobes (Fig. 2A–C). The electron density map showed that the activation loop region of npMAP2K6/AMP-PNP configured three novel short α-helices (Fig. 2A and D) that wrap around the tri-phosphate moiety of AMP-PNP (Fig. 2B). These helices correspond to amino acids 200–205, 207–213 and 222–226, and are referred to as activation helix-1 (AH1), activation helix-2 (AH2) and activation helix-3 (AH3), respectively (Fig. 2D). The C-terminal DVD domain (residues 311–334) in the npMAP2K6/AMP-PNP complex includes the two αJ- and αK-helices and is embraced by the C-lobe. The DVD domain plays a crucial role in the binding of MAP3K3. The structural details of the npMAP2K6/AMP-PNP complex provide important information about the putative regulatory mechanism of MAP2K6 auto-inhibition (see below).

N-terminal region of npMAP2K6

The npMAP2K6/AMP-PNP structure is the first reported full-length structure of MAP2Ks. The N-terminal region of npMAP2K6, including the D domain (residues 1–15) and a short stretch located close to the N-terminus (residues 16–43), possibly corresponds to the NRD (residues 44–58) of non-phosphorylated MAP2K1 (npMAP2K1), which is known to be fully disordered. The disordered D domain of MAP2K6 is known to be important for correct recognition and in facilitating signal transduction of p38 MAP kinase (*37*). Therefore, we speculate that the D domain is intrinsically disordered and undergoes a transition to an ordered state on binding to p38 kinases.

The short stretch sequence equivalent to NRD in npMAP2K1 was disordered in the npMAP2K6/AMP-PNP complex. In the auto-inhibition state of npMAP2K1, the NRD region adopts an α-helix and forms hydrogen bonds and hydrophobic interactions with the β4-sheet and αC–β4 loop. These interactions induce the movement of the β4-sheet towards the NRD region and subsequently block the αC-helix movement towards the ATP binding pocket (*24*). The flexibility in the short stretch of npMAP2K6 suggests that the region lacks a role as a NRD and solely operates as a flexible linker connecting the D domain and the kinase domain. It is conceivable that the flexibility of this short stretch increases the chances of an interaction between the MAP2K6 and p38 MAP kinases. Therefore, it is likely that an alternative stabilization mechanism for the auto-inhibition state of npMAP2K6 exists, and that this mechanism is different than the mechanism used by npMAP2K1.

ATP binding site of npMAP2K6

The AMP-PNP molecule bound to the ATP binding site is in the canonical state (Fig. 2C). The adenine moiety of AMP-PNP is anchored by four hydrogen bonds with Met129, Glu130 and Met132 in the hinge region of npMAP2K6. The 6-amino group of the adenine moiety forms two hydrogen bonds with the backbone carbonyl oxygen of Glu130 and the Sδ atom of Met129. Other hydrogen bonds are formed between the N1 and C2 atoms of the adenine moiety and the backbone NH and carbonyl oxygen of Met132, respectively. The adenine moiety of AMP-PNP is also situated in the hydrophobic pocket at the ATP binding cleft, and consists of several hydrophobic residues: Leu59, Val67, Ala80, Val113, Met129, Leu131, Met132 and Leu186. The tri-phosphate moiety binds to npMAP2K6 via several hydrogen and coordinate bonds. The three oxygen atoms from each phosphate group of AMP-PNP coordinate with the Mg^{2+} ion ligated by Asn184 and Asp197. The α- and γ-phosphate groups make hydrogen bonds with Lys82, a residue essential to kinase activity. The β-phosphate group forms a hydrogen bond with Ser183. The γ-phosphate group is fixed by three hydrogen bonds with two lysine residues Lys181 and Lys210, and Asp179; a residue working as the proton acceptor that is activated by the substrate hydroxyl group (Fig. 2C and D).

The conformation of the tri-phosphate moiety in the npMAP2K6/AMP-PNP complex is conserved in the npMAP2K1 complexed with ATP-γS (*24*) (Fig. 3A), but is distinguishable from the active Akt ternary complex with AMP-PNP and the GSK3β-peptide (Akt/AMP-PNP/GSK) (*22*) (Fig. 3B). In particular, while

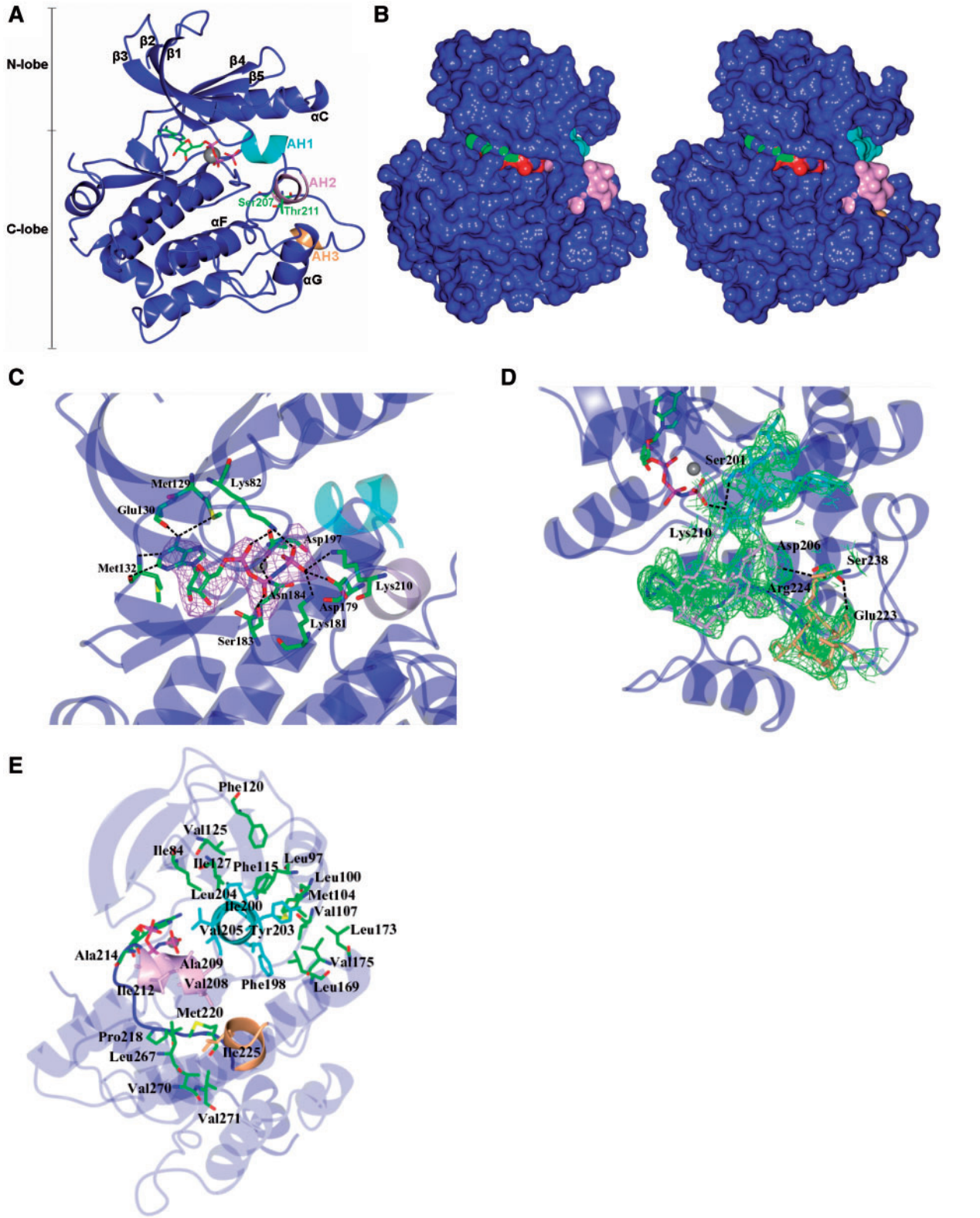

Fig. 2 Structure of the npMAP2K6/AMP-PNP complex. (A) One MAP2K6 monomer in the asymmetric unit is coloured blue, and AH1, AH2 and AH3 are coloured cyan, pink and orange, respectively. The protein is represented as a ribbon diagram. Mg^{2+} is indicated by a grey sphere, and AMP-PNP is shown using a ball and stick diagram. The phosphorylation site at Ser207 and Thr211 is shown in detail. (B) A stereo view of the molecular surface representation of npMAP2K6/AMP-PNP. The npMAP2K6/AMP-PNP is coloured blue, and AH1, AH2 and AH3 are coloured cyan, pink and orange, respectively. (C) The $F_o - F_c$ map at 3σ level revealed that the AMP-PNP molecule bound to the ATP binding cleft between the N and C lobes. The AMP-PNP and key residues for AMP-PNP binding are shown in a ball and stick representation. Hydrogen bonds for AMP-PNP bindings are drawn as dotted lines. (D) The $2F_o - F_c$ map contoured at 1.5σ covers the AH1, AH2 and AH3. Key residues for activation helix positioning are shown in the ball and stick representation. Hydrogen bonds are indicated by dotted lines. (E) The hydrophobic core formation allows the activation helices to be tethered to the kinase main body of npMAP2K6.

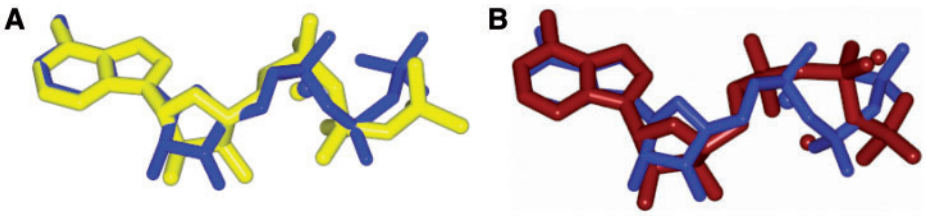

Fig. 3 Conformational comparisons of the ATP analogues binding to the kinases. (A) Superimposed AMP-PNP of npMAP2K6/AMP-PNP (blue) and ATP-γS of npMAP2K1/ATM (yellow). (B) Superimposed AMP-PNP of npMAP2K6/AMP-PNP (blue) and AMP-PNP of Akt/AMP/GSK (tan). In npMAP2K6/AMP-PNP, the tri-phosphate moiety was in a different conformation when compared with npMAP2K1/ATP and Akt/AMP/GSK.

the γ-phosphate group in the Akt/AMP-PNP/GSK complex is exposed to the bulk solvent and comes close to the phosphorylation residue Ser9 of the substrate GSK3β (*22*), the γ-phosphate group in the npMAP2K6/AMP-PNP complex is entirely concealed by the active site residues (Fig. 2B–D). Consequently, the AMP-PNP conformation in the npMAP2K6/AMP-PNP complex is likely to represent an inactive state.

The activation loop region of npMAP2K6

The activation loop region in the npMAP2K6/AMP-PNP complex forms three helices, referred to as AH1, AH2 and AH3 (Fig. 2A and D). These helices represent a novel conformation for this region. These activation helices are positioned by a hydrogen-bond relay between each other, AMP-PNP or the kinase main body. AH1 interacts with AH2 by a hydrogen bond of the Oγ atom of Ser201 with the Nζ atom of Lys210, and these atoms are concomitant donors to form hydrogen bonds with the γ-phosphate group of AMP-PNP. AH2 was fixed by AH3 via a hydrogen bond between the Oδ atom of Asp206 and the Nη atom of Arg224. AH3 was tethered by the αF-helix via a hydrogen bond between the Oγ atom of Ser238 and the Oε atom of Glu223. Furthermore, the activation helices were anchored by the kinase main body through the participation of two hydrophobic clusters (Fig. 2E). Phe198, Ile200, Tyr203, Leu204 and Val205 in AH1 formed one large hydrophobic cluster cooperating with Ile84, Leu97, Leu100, Met104, Val107, Phe115, Phe120, Val125, Ile127, Leu169, Leu173 and Val175 in the β3-, β4- and β5-strands, and αC- and αE helices of the main body of the kinase. Val208, Ala209 and Ile212 in AH2, Ile225 in AH3, and Ala214, Pro218 and Met220 in the AH2–AH3 loop, and Leu267, Val270 and Val271 in the αG-helix formed the other hydrophobic cluster. Through the formation of these hydrogen bonds and hydrophobic clusters, the activation helices probably contribute to the conformational stability of npMAP2K6, whereas in the active mutant MAP2K6-DD, these regions are flexible (*23*).

The putative auto-inhibition to activation mechanism of MAP2K6

The crystal structures of the npMAP2K6/AMP-PNP complex and apo-MAP2K6-DD disclose a putative auto-inhibition to activation mechanism of MAP2K6 (Fig. 4). The inactive npMAP2K6 inhibits a structural

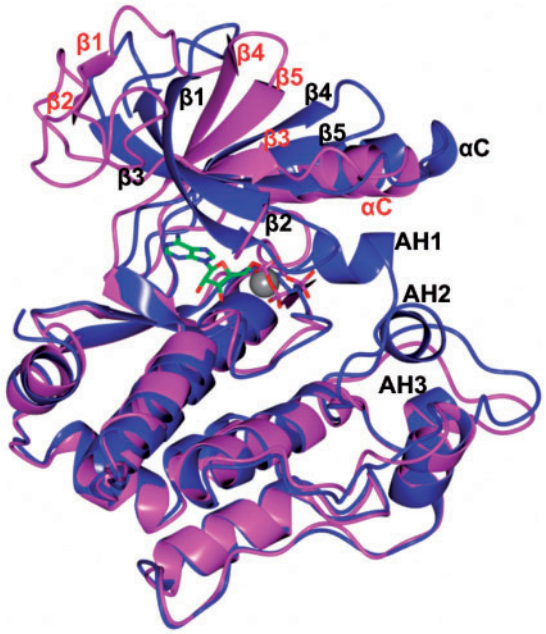

Fig. 4 Superimposed image of npMAP2K6/AMP-PNP (blue) on apo-MAP2K6-DD (magenta). The N-terminal lobe of apo-MAP2K6-DD is partially unwound. The unwound part of β1 and β2 form a large β1–β2 loop. In contrast, npMAP2K6 has structured β-strands, but not the extended loop.

re-configuration that is fundamental in the conversion to the active state. The αC-helix, a vital participant in the active state, was positioned distal from the active site and formed part of the large hydrophobic cluster that also included AH1, the β3-, β4- and β5-strands and the αE-helix. Moreover, the γ-phosphate group of AMP-PNP was enclosed by AH1 and AH2, which were tethered by several hydrophilic and hydrophobic interactions with the main body of MAP2K6 (Fig. 2B). Therefore, the conformation of the npMAP2K6/AMP-PNP complex most likely represents an auto-inhibition state.

The phosphorylation at Ser207 and Thr211 in AH2, which form hydrogen bonds with Asp179 and Cys216 in the npMAP2K6/AMP-PNP complex, allows the activation helices to detach from the main body of MAP2K6. This state was probably manifested by the apo-structure of the active mutant MAP2K6-DD (*23*). The disordered activation loop region and the detachment of the αC-helix from the hydrophobic cluster are likely to facilitate the transition of the

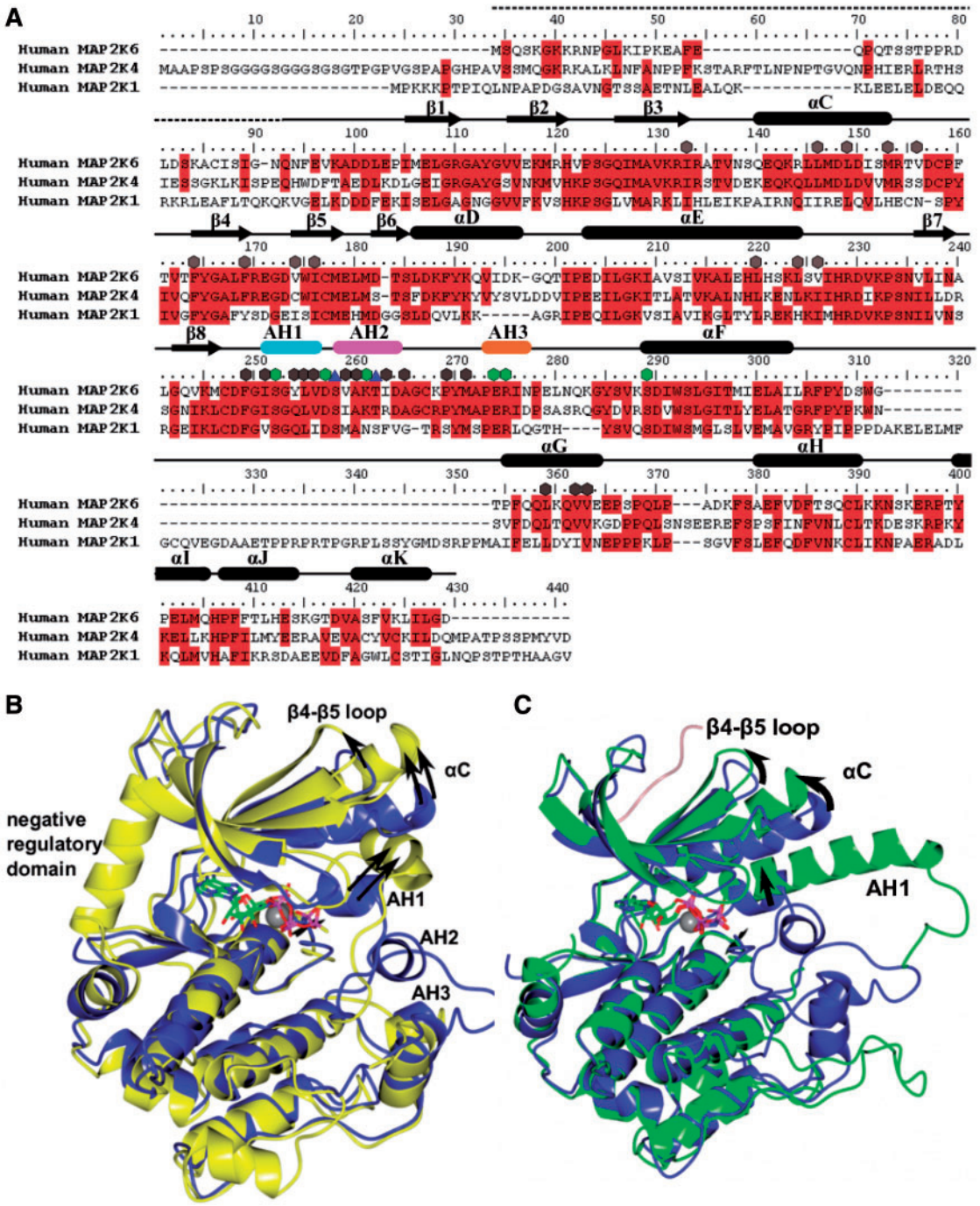

Fig. 5 Comparison of the npMAP2K6/AMP-PNP structure with the npMAP2K1/ATP and npMAP2K4/AMP/p38 structures. (A) Sequence alignment of MAP2K6, MAP2K4 and MAP2K1. Strictly conserved residues are highlighted with a red background. The secondary structure from MAP2K6 is shown above the alignment. The secondary structural motifs for MAP2K6 are indicated by arrows for β-strands, cylinders for α-helices, lines for coils or turns and dot line for disorder. The AH1, AH2 and AH3 are coloured cyan, pink and orange, respectively. The phosphorylation residues in the activation loop are denoted with blue triangles. The residues responsible for auto-inhibition are indicated by green hexagon for hydrogen bonds and grey hexagons for hydrophobic interactions. Alignments were performed using ClustalW (*38*). (B) Superimposition of npMAP2K6/AMP-PNP to npMAP2K1/ATP. The npMAP2K6/AMP-PNP is coloured blue and npMAP2K1/ATP is coloured yellow. AH1 in npMAP2K1/ATP is distal from the ATP binding pocket when compared with npMAP2K6/AMP-PNP. (C) Superimposed image of npMAP2K6/AMP-PNP on npMAP2K4/AMP/p38. The npMAP2K6/AMP-PNP is coloured blue and npMAP2K4/AMP/p38 is coloured green. The p38 peptide (pink) is shown as a ribbon diagram. AH1 in npMAP2K4 and npMAP2K6 begins at the first residue of the activation loop and blocks the access of the substrate or inhibitor to the ATP binding pocket.

apo-MAP2K6-DD to the active configuration. Finally, ATP binding to the active site may raise the fully active conformation of MAP2K6; although that structure has not been reported.

Comparison of inactivation mechanism of MAP2K6 with other inactivation mechanisms found in MAP2Ks

MAP2K6 and MAP2K1 have distinct auto-inhibition mechanisms, although both npMAP2Ks resemble each

other structurally. AH1 and AH2 of npMAP2K6 encompass the γ-phosphate group of ATP (Figs 2A–D and 5A) and consequently contribute to the formation of the auto-inhibition state. The activation loop region of npMAP2K1 also contains two short α-helices, corresponding to AH1 and AH3 in npMAP2K6. However, because of the NRD, the AH1 region along with the αC-helix of npMAP2K1 is shifted outwards from the active site when compared with npMAP2K6 (Fig. 5B). The resultant shift confers a large space proximal to the γ-phosphate group of ATP-γS in the npMAP2K1/ATP-γS complex, which is accessible to the solvent. A crystal structure showed that the ATP-non-competitive inhibitor of MAP2K1 bound to this solvent-accessible space in conjunction with ATP binding and formed a hydrogen bond with the γ-phosphate group of ATP (*37*). AH1 of npMAP2K6 plays a dominant contribution to the fixing of the γ-phosphate group of ATP, whereas this helix in npMAP2K1 plays a negligible role in the binding of ATP.

The crystal structures of npMAP2K4 (*25*) depicted a substrate-dependent inactivation mechanism apparently different from that observed for npMAP2K6. The activation loop region of the npMAP2K6/AMP-PNP complex configured three short α-helices that are significant in forming the auto-inhibition state, whereas this region in the npMAP2K4/AMP-PNP complex was largely disordered (*25*). Binding of the p38 peptide to the npMAP2K4/AMP-PNP complex (npMAP2K4/AMP-PNP/p38) allowed npMAP2K4 to shift to an inactive state configuring a long α-helix corresponding to AH1 in npMAP2K6 (Fig. 5A and C) (*25*). The p38 peptide interacted with the β4–β5 loop along with the αC-helix and AH1 of npMAP2K4, as well as the NRD of MAP2K1 (Fig. 5B and C), and probably prevents npMAP2K4 changing to the active conformation. A line of shifts rendered a small space around the γ-phosphate group in the npMAP2K4/AMP-PNP/p38 complex. Conversely, in the npMAP2K6/AMP-PNP complex, there is no space around the γ-phosphate group, which forms hydrogen bonds with AH1 and AH2.

The npMAP2K6 appears to adopt a novel auto-inhibition mechanism, enclosing the γ-phosphate group by a molecular wall consisting of the AH1 and AH2 regions of the protein that are fixed to the main body via hydrophobic interactions. Such a mechanism is different from those observed for npMAP2K1 and npMAP2K4 regulation.

Conclusions

The crystal structure of the npMAP2K6/AMP-PNP complex was successfully obtained via buffer optimization using Native–PAGE and DLS experiments. The structure depicts the auto-inhibition machinery of MAP2K6. The npMAP2K6, displaying extremely low activity, was stabilized in the inactive conformation by several interactions between residues in the activation loop region, which formed three short α-helices (AH1, AH2 and AH3), and residues in the main body of kinase domain. The results show that the molecular brake of npMAP2K6 involves a pair of α-helices, AH1 and AH2. This is because these helices conceal the γ-phosphate of ATP when the protein is in the inactive conformation. The phosphorylation in AH2 of npMAP2K6 presumably releases the molecular brake and triggers a conformational transition to the flexible state as observed in the apo-structure of the active mutant MAP2K6-DD.

The molecular brake of npMAP2K6 is different from that of npMAP2K1 or npMAP2K4, which fix the N-lobe motion along with the αC-helix by the NRD (residues 44–58) and the p38 peptide, respectively.

Acknowledgements

We thank A. Yamano for discussions, advice and critical reading. We also thank the beamline staff at KEK-PF BL-5A for data collection.

Funding

PharmAxess, Inc., Akishima, Tokyo.

Conflict of interest

None declared.

References

1. Raman, M., Chen, W., and Cobb, M.H. (2007) Differential regulation and properties of MAPKs. *Oncogene* **26**, 3100–3112
2. Chen, Z., Gibson, T.B., Robinson, F., Silvestro, L., Pearson, G., Xu, B., Wright, A., Vanderbilt, C., and Cobb, M.H. (2001) MAP kinases. *Chem. Rev.* **101**, 2449–2476
3. Chang, L. and Karin, M. (2001) Mammalian MAP kinase signalling cascades. *Nature* **410**, 37–40
4. Avruch, J., Zhang, X.-F., and Kyriakis, J.M. (1994) Raf meets Ras: completing the framework of a signal transduction pathway. *Trends Biochem. Sci.* **19**, 279–283
5. Davis, R.J. (1993) The mitogen-activated protein kinase signal transduction pathway. *J. Biol. Chem.* **268**, 14553–14556
6. Davis, R.J. (2000) Signal transduction by the JNK group of MAP kinases. *Cell* **103**, 239–252
7. Cuenda, A. (2000) Mitogen-activated protein kinase kinase 4 (MKK4). *Int. J. Biochem. Cell Biol.* **32**, 581–587
8. Robinson, V.L., Hickson, J.A., Vander Griend, D.J., Dubauskas, Z., and Rinker-Schaeffer, C.W. (2003) MKK4 and metastasis suppression: a marriage of signal transduction and metastasis research. *Clin. Exp. Metastasis* **20**, 25–30
9. Cuenda, A., Rouse, J., Doza, Y.N., Meier, R., Cohen, P., Gallagher, T.F., Young, P.R., and Lee, J.C. (1995) SB 203580 is a specific inhibitor of a MAP kinase homologue which is stimulated by cellular stresses and interleukin-1. *FEBS Lett.* **364**, 229–233
10. Hickson, J.A., Huo, D., Vander Griend, D.J., Lin, A., Rinker-Schaeffer, C.W., and Yamada, S.D. (2006) The p38 kinases MKK4 and MKK6 suppress metastatic colonization in human ovarian carcinoma. *Cancer Res.* **66**, 2264–2270
11. Whitmarsh, A.J. and Davis, R.J. (1996) Transcription factor AP-1 regulation by mitogen-activated protein

kinase signal transduction pathways. *J. Mol. Med.* **74**, 589–607

12. Raingeaud, J., Whitmarsh, A.J., Barrett, T., Derijard, B., and Davis, R.J. (1996) MKK3- and MKK6-regulated gene expression is mediated by the p38 mitogen-activated protein kinase signal transduction pathway. *Mol. Cell Biol.* **16**, 1247–1255
13. Moriguchi, T., Kuroyanagi, N., Yamaguchi, K., Gotoh, Y., Irie, K., Kano, T., Shirakabe, K., Muro, Y., Shibuya, H., Matsumoto, K., Nishida, E., and Hagiwara, M. (1996) A novel kinase cascade mediated by mitogen-activated protein kinase kinase 6 and MKK3. *J. Biol. Chem.* **271**, 13675–13679
14. Han, J., Lee, J.D., Jiang, Y., Li, Z., Feng, L., and Ulevitch, R.J. (1996) Characterization of the structure and function of a novel MAP kinase kinase (MKK6). *J. Biol. Chem.* **271**, 2886–2891
15. Stein, B., Brady, H., Yang, M.X., Young, D.B., and Barbosa, M.S. (1996) Cloning and characterization of MEK6, a novel member of the mitogen-activated protein kinase kinase cascade. *J. Biol. Chem.* **271**, 11427–11433
16. Widmann, C., Gibson, S., Jarpe, M.B., and Johnson, G.L. (1999) Mitogen-activated protein kinase: conservation of a three-kinase module from yeast to human. *Physiol. Rev.* **79**, 143–180
17. Enslen, H., Raingeaud, J., and Davis, R.J. (1998) Selective activation of p38 mitogen-activated protein (MAP) kinase isoforms by the MAP kinase kinases MKK3 and MKK6. *J. Biol. Chem.* **273**, 1741–1748
18. Jiang, Y., Gram, H., Zhao, M., New, L., Gu, J., Feng, L., Di Padova, F., Ulevitch, R.J., and Han, J. (1997) Characterization of the structure and function of the fourth member of p38 group mitogen-activated protein kinases, p38delta. *J. Biol. Chem.* **272**, 30122–30128
19. Bardwell, A.J., Abdollahi, M., and Bardwell, L. (2003) Docking sites on mitogen-activated protein kinase (MAPK) kinases, MAPK phosphatases and the Elk-1 transcription factor compete for MAPK binding and are crucial for enzymic activity. *Biochem. J.* **370**, 1077–1085
20. Bardwell, L. (2006) Mechanisms of MAPK signalling specificity. *Biochem. Soc. Trans.* **34**, 837–841
21. Takekawa, M., Tatebayashi, K., and Saito, H. (2005) Conserved docking site is essential for activation of mammalian MAP kinase kinases by specific MAP kinase kinase kinases. *Mol. Cell* **18**, 295–306
22. Yang, J., Cron, P., Good, V.M., Thompson, V., Hemmings, B.A., and Barford, D. (2002) Crystal structure of an activated Akt/protein kinase B ternary complex with GSK3-peptide and AMP-PNP. *Nat. Struct. Biol.* **9**, 940–944
23. Min, X., Akella, R., He, H., Humphreys, J.M., Tsutakawa, S.E., Lee, S.J., Tainer, J.A., Cobb, M.H., and Goldsmith, E.J. (2009) The structure of the MAP2K MEK6 reveals an autoinhibitory dimmer. *Structure* **17**, 96–104
24. Fischmann, T.O., Smith, C.K., Mayhood, T.W., Myers, J.E., Reichert, P., Mannarino, A., Carr, D., Zhu, H., Wong, J., Yang, R.S., Le, H.V., and Madison, V.S. (2009) Crystal structures of MEK1 binary and ternary complexes with nucleotides and inhibitors. *Biochemistry.* **31**, 2661–2674
25. Matsumoto, T., Kinoshita, T., Kirii, Y., Yokota, K., Hamada, K., and Tada, T. (2010) Crystal structures of MKK4 kinase domain reveal that substrate peptide binds to an allosteric site and induces an auto-inhibition state. *Biochem. Biophys. Res. Commun.* **400**, 369–373
26. Collaborative Computational Project, Number 4. (1994) The CCP4 Suite: programs for protein crystallography. *Acta Crystallogr.* **D50**, 760–763
27. Vagin, A. and Teplyakov, A. (1997) A. MOLREP: an automated program for molecular replacement. *J. Appl. Crystallogr.* **30**, 1022–1025
28. Emsley, P. and Cowtan, K. (2004) Coot: model-building tools for molecular graphics. *Acta Crystallogr.* **D60**, 2126–2132
29. Murshudov, G.N., Vagin, A.A., and Dodson, E.J. (1997) Refinement of macromolecular structures by the maximum-likelihood method. *Acta Crystallogr.* **D53**, 240–255
30. Adams, P.D., Afonine, P.V., Bunkóczi, G., Chen, V.B., Davis, I.W., Echols, N., Headd, J.J., Hung, L.-W., Kapral, G.J., Grosse-Kunstleve, R.W., McCoy, A.J., Moriarty, N.W., Oeffner, R., Read, R.J., Richardson, D.C., Richardson, J.S., Terwilliger, T.C., and Zwart, P.H. (2010) PHENIX: a comprehensive Python-based system for macromolecular structure solution. *Acta Crystallogr* **D66**, 213–221
31. Krissinel, E. and Henrick, K. (2004) Secondary-structure matching (SSM), a new tool for fast protein structure alignment in three dimensions. *Acta Crystallogr.* **D60**, 2256–2268
32. Potterton, L., McNicholas, S., Krissinel, E., Gruber, J., Cowtan, K., Emsley, P., Murshudov, G.N., Cohen, S., Perrakis, A., and Noble, M. (2004) Developments in the CCP4 molecular-graphics project. *Acta Crystallogr.* **D60**, 2288–2294
33. Kinoshita, T., Miyano, N., Nakai, R., Yokota, K., Ishiguro, H., and Tada, T. (2008) Protein purification and preliminary crystallographic analysis of human Lyn tyrosine kinase. *Protein Expr. Purif.* **58**, 318–324
34. Deacon, K. and Blank, J.L. (1999) MEK kinase 3 directory activated MKK6 and MKK7, specific activators of the p38 and c-Jun NH2-terminal kinases. *J. Biol. Chem.* **274**, 16604–16610
35. Bernstein, B.E., Michels, P.A., Kim, H., Petra, P.H., and Hol, W.G. (1998) The importance of dynamic light scattering in obtaining multiple crystal forms of Trypanosoma brucei PGK. *Protein Sci.* **7**, 504–507
36. Ferré-D'Amaré, A.R. and Burley, S.K. (1994) Use of dynamic light scattering to assess crystallizability of macromolecules and macromolecular assemblies. *Structure* **2**, 357–359
37. Iversion, C., Larson, G., Lai, C., Yain, L.T., Dadson, C., Weingarten, P., Appleby, T., Vo, T., Maderna, A., Vernier, J.M., Hamatake, R., Miner, J.N., and Quart, B. (2009) RDEA119/BAY869766: A potent, selective, allosteric inhibitor of MEK1/2 for the treatment of cancer. *Cancer Res.* **69**, 6839–6847
38. Thompson, J.D., Higgins, D.G., and Gibson, T.J. (1994) CLUSTAL W: Improving the sensitivity of progressive multiplesequence alignment through sequence weighting, position-specificgap penalties and weight matrix choice. *Nucleic Acids Res.* **22**, 4673–4680